ChemCatChem

Research Article
doi.org/10.1002/cctc.202400945

Chemistry Europe
European Chemical Societies Publishing

www.chemcatchem.org

Modular Assembly and Optimization of an Artificial Esterase from Functionalised Surfactants

Olivia Matich,[a, b] Mohinder Maheshbhai Naiya,*[a, b] Joanne Salam,[a] Bryan Andres Tiban Anrango,[a] and Jack L.-Y. Chen*[a, b, c]

A strategy for the screening and optimization of an artificial esterase is presented that utilizes the self-assembly of amphiphilic molecules. Unlike conventional approaches that rely on the attachment of key functional groups onto molecular scaffolds or surfaces, the modular assembly of amphiphiles allows a large number of catalytic combinations to be investigated with minimal synthetic effort. In this study, iterative combinatorial screens led to an optimized esterase comprising amphiphiles that act as a nucleophilic catalyst, an oxyanion hole and a metal ion chelator. Cooperativity is observed between the functional headgroups of the amphiphiles, an effect that is diminished when co-assembled with non-functionalized surfactants. Assessment of the catalytic efficiency (k_{cat}/K_M) of our optimized catalysts against recently reported artificial esterases shows comparable efficiency, indicating that efficient catalysis is possible with dynamic self-assembled systems despite the absence of pre-defined rigid binding pockets.

Introduction

The remarkable properties of nature's enzymes are essential not only for cellular function but are increasingly being explored for industrial applications.[1,2] Their extraordinary efficiency stems from the ability to position key functional groups around an active site, with an arrangement that permits the groups to act synergistically in the acceleration of a chemical reaction.[3,4] Enzymes achieve this through protein folding, which enables the formation of unique three-dimensional structures that position the requisite amino acid residues into the optimum configuration to catalyze a chemical reaction. This process is highly effective in controlled environments, but the practical utility of enzymes for industrial applications is significantly limited by the sensitivity of protein folding to changes in pH, temperature, ionic strength, or the addition of organic solvents.[5]

A long-standing aim for enzyme mimicry has been the construction of model catalytic systems with improved stability and reactivity.[6,7] Conventional approaches involve the identification of the key functional groups required for catalysis and their placement onto a scaffold (Figure 1a), with emphasis on the concepts of confinement, rigid binding pockets, and restricted rotation of the bound substrate. Examples include the attachment of the requisite groups onto molecular scaffolds such as cyclodextrins, cucurbiturils and cavitands,[8–14] onto dendrimers[15,16] and onto the surfaces of nanoparticles and

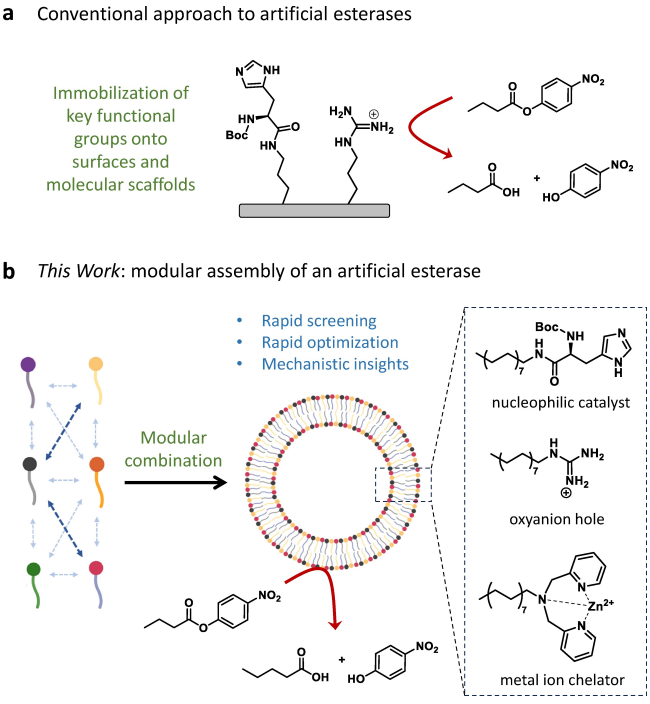

Figure 1. Representation of a) an artificial esterase formed from the co-immobilization of requisite functional groups onto a molecular scaffold or solid support and b) an artificial esterase formed from the co-assembly of amphiphiles. The modular nature of the self-assembled catalyst system enables rapid screening of amphiphile combinations, allowing for facile catalyst optimization and investigation of the reaction mechanism.

[a] O. Matich, M. M. Naiya, J. Salam, B. A. Tiban Anrango, J. L.-Y. Chen
School of Science, Auckland University of Technology, Auckland 1142, New Zealand
E-mail: jack.chen@aut.ac.nz

[b] O. Matich, M. M. Naiya, J. L.-Y. Chen
The MacDiarmid Institute for Advanced Materials and Nanotechnology, Victoria University of Wellington, Wellington 6011, New Zealand

[c] J. L.-Y. Chen
Department of Biotechnology, Chemistry and Pharmaceutical Sciences, Università degli Studi di Siena, 53100 Siena, Italy

Supporting information for this article is available on the WWW under https://doi.org/10.1002/cctc.202400945

polymers.[17–20] While such systems can be effective enzyme mimics, catalyst optimization can be a challenging process, where modification of a functional group, or their specific position within the scaffold, requires the complete re-synthesis of the entire catalyst.

To overcome these challenges, an increasing number of research groups are taking an alternative approach and forming enzyme mimics by self-assembly. Examples include the assembly of amino acids and short peptides to form supramolecular assemblies such as hydrogels,[21,22] nanofibers,[23–27] and nanotubes.[28,29] DeGrado, Korendovych and co-workers have described the formation of Zn^{2+}-dependent esterases by the self-assembly of heptapeptides into amyloid fibrils,[30] while Gazit and co-workers demonstrated that even single amino acids can coordinate with Zn^{2+} ions to form amyloid structures with esterase activity.[31] Important contributions have also been made by Zhao and co-workers using templated polymerization of micellar assemblies to produce molecularly imprinted nanoparticles.[32–34] Each of these examples relies on the self-assembly of small building blocks to form supramolecular structures with conformationally rigid catalytic pockets. Perhaps more surprising are reports of the self-assembly of amphiphiles to form catalytic pockets within micellar and vesicular structures where cooperativity occurs intermolecularly between functional groups on proximal polar head groups.[35–39] These systems describe enhancement in catalytic activity that can be directly attributed to cooperative effects between functionalized amphiphiles,[40–44] rather than conventional micellar effects where rate accelerations are generally attributed to concentration enhancement, or local changes in pH.[45–48] Connal and co-workers have shown that an amphiphile containing the His-Asp-Ser catalytic triad can be co-assembled with a second amphiphile containing a guanidinium head group to achieve enhanced esterase activity.[49,50] Our group have shown that Zn^{2+}-binding amphiphiles can be co-assembled with guanidinium-containing amphiphiles to form artificial phosphodiesterases.[35] These micellar and vesicular assemblies differ from the examples of artificial enzymes described above, in that the supramolecular structures are highly dynamic, and do not rely on the formation of well-defined rigid binding pockets. Unlike the formation of hydrogels or nanofibrils, micellar and vesicular assemblies do not require a specific amino acid sequence in their building blocks to code for their assembly. Any polar functional group could potentially be turned into an amphiphile by attachment of a hydrophobic tail and be co-assembled with other amphiphiles to explore the formation of cooperative interactions. This greatly increases the number of synergistic combinations that can be rapidly investigated, giving it potential to be a platform for catalyst discovery and optimization. Herein, we demonstrate these concepts in the rapid screening and optimization of an artificial esterase, and to obtain insight into the mechanism of esterolysis within the self-assembled system with minimal synthetic effort.

Results and Discussion

We began by attempting to re-create the His-Asp-Ser catalytic triad, by combining amphiphiles containing each of the key functional groups present in the three amino acids. Palmitic acid (**P**) was used to introduce the carboxylic acid functional group into the assembly, while commercially available detergent Brij® O10 (**B**) was used to provide the hydroxyl group. An amphiphilic derivative of histidine was synthesized beginning from τ-benzyl-*N*$^{\alpha}$-(*tert*-butoxycarbonyl)-L-histidine (**1**), which was treated with HBTU to form an activated ester that was directly reacted with hexadecyl amine to form amide **2a** (Scheme 1). Benzyl deprotection via hydrogenation furnished the desired histidine-containing amphiphile **H**. The α-amino group was retained as the protected carbamate as this amino group would form part of the main polypeptide chain in the native enzyme. An analogous histidine-containing amphiphile with a C_4-alkyl chain (**3**) was also synthesized to act as a control molecule for subsequent experiments.

Amphiphile **G** was of interest due to the prevalent use of the guanidinium group in artificial systems to simulate an oxyanion hole, owing to its ability to donate strong, bifurcated H-bonding interactions with carbonyl groups, enhancing substrate binding and facilitating catalysis.[49,51,52] The route to the guanidinium amphiphile began with the coupling of hexadecylamine with an electrophilic source of guanidine (1,3-di-Boc-2-(trifluoromethylsulfonyl)guanidine, **4**) to form guanidine **5a** (Scheme 1). Removal of the Boc protecting groups using HCl afforded the desired amphiphile **G** containing a C_{16}-chain.

The esterolysis activity of the individual amphiphiles and their combinations were examined in aqueous solution at pH 7.0 ([HEPES] = 5 mM) in the presence of excess substrate *p*-nitrophenyl butyrate (**PNPB**; Figure 2). **PNPB** is an ideal model substrate as it possesses greater hydrolytic stability than the commonly used *p*-nitrophenyl acetate, and its hydrolysis releases *p*-nitrophenol (**PNP**), which allows the reaction to be

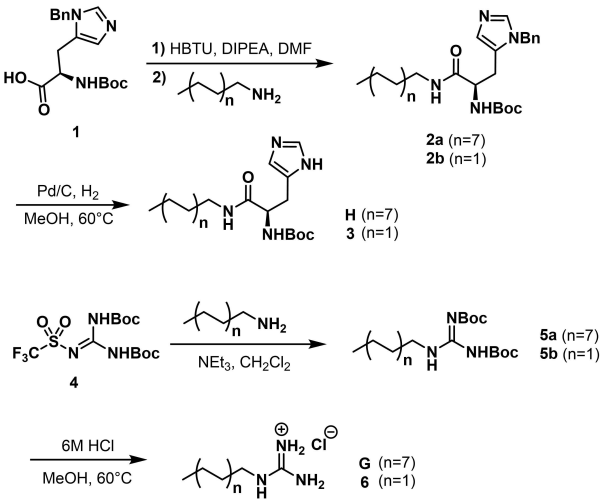

Scheme 1. Synthesis of the amphiphile C_{16}-histidine **H** and the control molecule C_4-histidine **3**. Synthesis of the amphiphile C_{16}-guanidinium **G** and the control molecule C_4-guanidinium **6**.

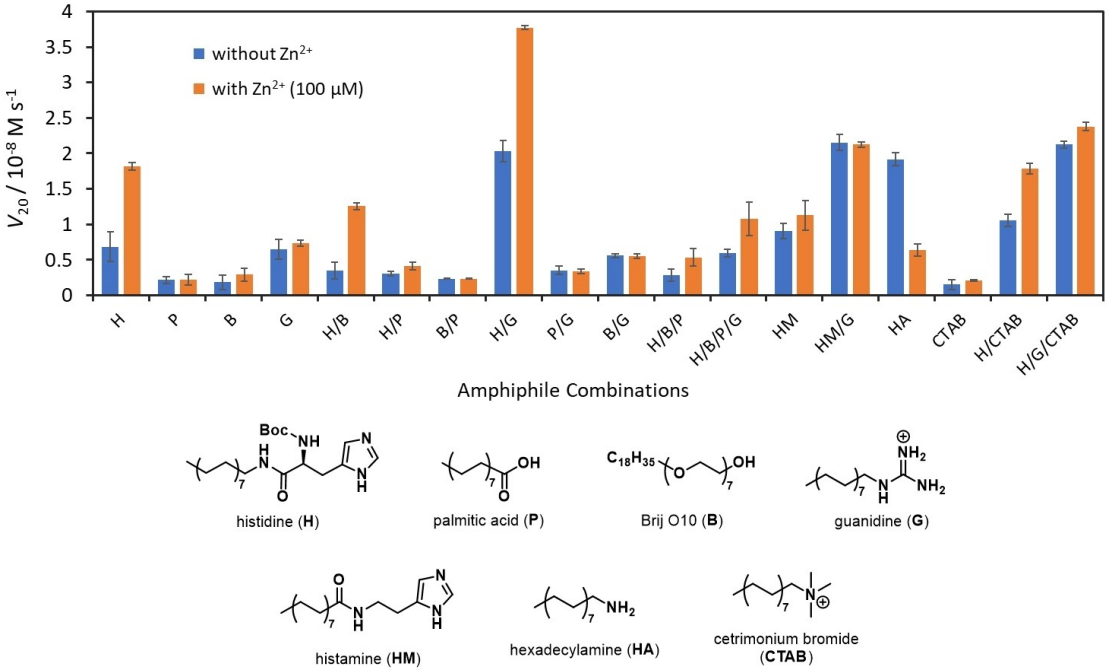

Figure 2. Rate of **PNPB** hydrolysis with different combinations of amphiphiles in the presence or absence of Zn^{2+}. Aqueous buffer pH = 7.0 ([HEPES] = 5 mM), [amphiphiles] = 100 μM, [**PNPB**] = 500 μM, 40 °C. V_{20} was compared rather than V_0 for this initial screen as the sample containing only **H** required time to stabilize (see Supporting Information, section 4ci).

followed spectrophotometrically by measuring the absorbance at 405 nm. Screening of catalytic activity was performed both in the absence and in the presence of Zn^{2+} ions, due to the myriad of examples where Zn^{2+} ions play a key role in the mechanism of esterolysis.[30,52] This initial screen showed that His-containing amphiphile **H** possessed moderate esterolysis activity on its own, with a marked enhancement of catalytic activity upon the addition of Zn^{2+} (Figure 2). The catalytic activity in the absence of Zn^{2+} is likely due to the ability of imidazole to act as a nucleophilic catalyst for esterolysis. The increased catalytic activity in the presence of Zn^{2+} is in line with reports that Zn^{2+} ions can be stabilized by three histidine residues in a tetrahedral array, which activates a fourth ligand, water and allows it to act as the nucleophile for esterolysis, a mechanism observed in the enzyme carbonic anhydrase.[53]

The esterolytic activity of the Asp-mimic (**P**) and Ser-mimic (**B**) were both low, while moderate activity was observed with the guanidylated amphiphile **G**. All possible pairings of the amphiphiles **H**, **P**, **B** and **G**, were subsequently screened, together with the catalytic triad-mimic **H**/**B**/**P**. The **H**/**G** combination, containing the imidazole and guanidinium groups, emerged as a clearly superior combination. Importantly, the observed catalytic activity for the **H**/**G** combination was over 2-fold greater than **H** on its own, and over 3-fold greater than the activity of **G** on its own, indicating a distinctive synergistic effect between the two amphiphiles. The activity of the amphiphiles **HM**, **HA**, **CTAB** and their combinations with the above amphiphiles were also examined and provided insight into the roles of each of the functional groups (see SI, section 4cii for details).

To investigate whether the observed enhancements in catalytic rate were due to cooperativity between the functional headgroups of the amphiphiles or a result of conventional micellar effects such as local pH changes, the **H**/**G** catalytic combination was examined within micellar matrices made up of either the non-ionic surfactant Brij® O10 (**B**) or the cationic surfactant **CTAB** (Supporting Information, Section 4d). The catalytic activity of 1 : 1 **H**/**G** (100 μM) in **B** (800 μM) (entry 4) was significantly higher than the activity observed with either **H** (100 μM) (entry 2) or **G** (100 μM) (entry 3) on their own in **B** (800 μM, blue bars), indicating the cooperative formation of catalytic pockets between **H** and **G** rather than synergistic effects due to the formation of aggregates. Interestingly, this rate is significantly lower than the rate of the 1 : 1 **H**/**G** (100 μM) system in the absence of **B** (orange bar, entry 13), due likely to the dilution of amphiphiles **H** and **G** within the **B** micellar matrix leading to a lower degree of **H**/**G** intermolecular cooperativity. For discussion on the effect of local pH changes due to the build-up of OH^- ions in the Stern layer, see Supporting Information, Section 4d).

While co-assembling amphiphiles within a micellar matrix can alleviate issues surrounding changes in structure of the self-assembled aggregates, this proved to be incompatible with the current study as co-micellization resulted in dilution of the intermolecular cooperative effects. As we were able to attain comparable catalytic activities while utilizing a much lower concentration of total amphiphiles, we proceeded to optimize the self-assembled system in the absence of non-functionalized surfactants. The modular nature of this self-assembled catalyst allowed the lead **H**/**G** combination to be easily optimized by modifying the ratio of **H** to **G** to probe the mechanism of the

reaction. Figure 3a shows how the rate of esterolysis changes with different ratios of **H** to **G**, both in the presence of Zn^{2+} (orange circles) and the absence of Zn^{2+} (blue circles). For both curves, there is clear evidence of cooperativity between the amphiphiles **H** and **G**, given that the activity of catalytic systems containing both **H** and **G** are always more efficient than when only **H** (far left) or only **G** (far right) is present. Further support for a cooperative mechanism is observed when **H** is replaced by its C4 analogue **3** (yellow circles) and **G** is replaced by its C4 analogue **6** (gray circles). In both cases, much reduced catalytic activity is observed, due to the inability of the control ligands **3** and **6** to form self-assembled structures where the catalytically active headgroups would be placed in close proximity.

For the self-assembled system in the absence of Zn^{2+} (blue circles), no distinctive peak in activity is observed at different ratios of **G** to **H**, while in the presence of Zn^{2+} (orange circles), a peak in activity was observed at 1:4 **H** to **G**. This result was somewhat surprising as it was expected that three **H** ligands were stabilizing a Zn^{2+}–OH_2 or Zn^{2+}–OH^- complex, while **G** activated the carbonyl in the substrate **PNPB** for nucleophilic attack. To further investigate the roles of **H** and **G** in the reaction, we measured the catalytic activity of the 1:4 **H/G** system in the presence of increasing Zn^{2+} concentrations. This experiment demonstrated an increase in the catalytic activity which plateaus at $[Zn^{2+}] = 25$ μM, which is ~equimolar to **H** and ~3 equivalent to **G**.

To probe whether the Zn^{2+} ions were being bound by the imidazole functional group in **H** or the guanidinium functional group in **G**, we determined the relative binding affinities of **H** and **G** to Zn^{2+} using the colorometric indicator pyrocatechol violet (PV, see SI, Section 4 g).[54,55] Titration of **H** to a solution containing 20 μM PV required 80 μM of **H** for the solution to change from yellow to blue. On the other hand, 20 μM of amphiphile **G** was sufficient to induce formation of a blue complex, indicating that **G** was able to bind Zn^{2+} more efficiently than **H**. Given the 3:1 stoichiometry between **G** and Zn^{2+}, as seen in Figure 3b, we propose that in this catalyst system, three guanidinium groups are involved in complexing each Zn^{2+} ion, similar to previous reports by Herres-Pawlis[56] and Sundermeyer.[57]

The lead 1:4 **H/G** catalyst system was further analyzed for its self-assembly properties. The critical aggregation concentration of the system was determined by the addition of the amphiphiles to a buffer solution containing 1,6-diphenyl-1,3,5-hexatriene (DPH), which estimated the critical aggregation concentration (CAC) to be 95 μM (Figure 4a). This was supported by a plot of the esterolysis rate vs total amphiphile concentration, for which a change in the slope was observed at ~100 μM total surfactant concentration (Figure 4b). Dynamic light scattering (DLS) determined the size of the aggregates to be predominantly in the 60–70 nm range (Figure 4c), which was

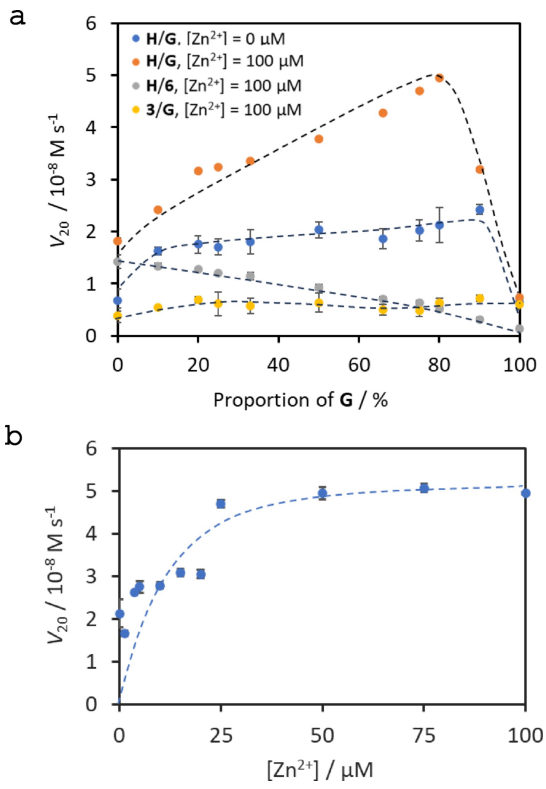

Figure 3. Optimization of the **H/G** catalyst system. (a) esterolysis rate at different ratios of **H/G** in the absence (blue circles) and presence of Zn^{2+} (orange circles) in aqueous buffer pH = 7.0 ([HEPES] = 5 mM), [amphiphiles] = 100 μM, [**PNPB**] = 500 μM, 40 °C; (b) esterolysis rate for 1:4 **H/G** at increasing concentrations of zinc, aqueous buffer pH = 7.0 ([HEPES] = 5 mM), [amphiphiles] = 100 μM, [**PNPB**] = 500 μM, 40 °C.

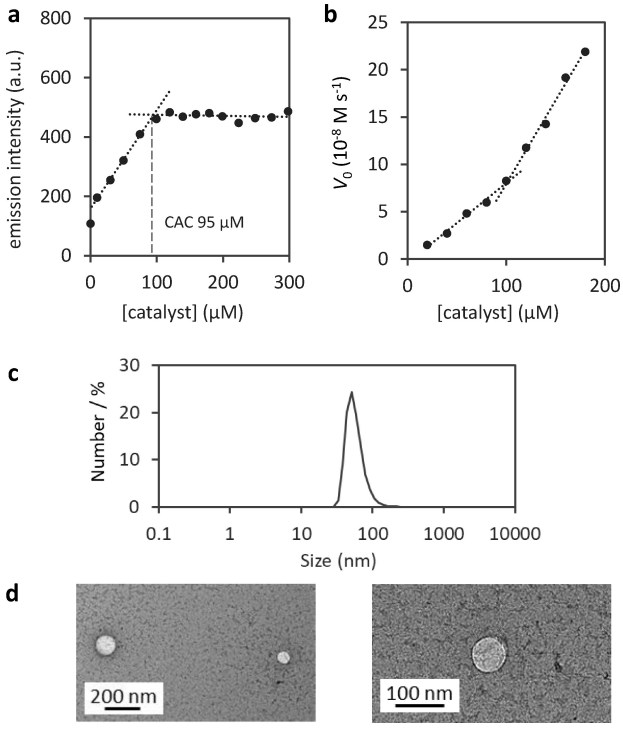

Figure 4. Analysis of the self-assembly properties for the 1:4 **H/G** catalyst system in the presence of Zn^{2+}. (a) fluorescence intensity of DPH at increasing catalyst concentrations to determine CAC, aqueous buffer pH = 7.0 ([HEPES] = 5 mM), [DPH] = 1 μM, [**PNPB**] = 500 μM, 40 °C; (b) esterolysis rate at increasing catalyst concentration, aqueous buffer pH = 7.0, ([HEPES] = 5 mM), [**PNPB**] = 500 μM, 40 °C; (c) DLS plot of 1:4 **H/G** catalyst (100 μM, $[Zn^{2+}] = 25$ μM) in aqueous buffer pH 7.0 ([HEPES] = 5 mM), [**PNPB**] = 500 μM; (d) representative TEM images of 1:4 **H/G** (200 μM) in aqueous buffer pH 7.0, ([HEPES] = 5 mM), $[Zn^{2+}] = 50$ μM, [PNPB] = 500 μM.

confirmed by imaging conducted with the electron microscope (Figure 4d).

Given our assumption that the role of three equivalents of **G** was to stabilize Zn^{2+}, we reasoned that our catalyst system could be further optimized by replacing the three equivalents of **G** with a stronger Zn^{2+} chelator. We thus performed a secondary optimization screen using amphiphiles featuring the well-known Zn^{2+}-chelating ligands 1,4,7-triazacyclononane and di-(2-picolyl)amine (Figure 5a).[58,59] The esterolytic activity of C_{16}-1,4,7-triazacyclononane (**TACN**) was first examined on its own, and found to exhibit a very high initial reaction rate which then plateaued after the conversion of approximately 20% of the substrate (see SI, Section 4i) This behavior suggested that the secondary amines in **TACN** were reacting with **PNPB** by direct nucleophilic attack in a non-catalytic manner, which was supported by the detection of high levels of **TACN**-butyrate adducts by mass analysis (SI, Section 4 h). The catalytic activity of **TACN** in the presence of Zn^{2+} was significantly reduced, as the **TACN**·Zn^{2+} complex would no longer be nucleophilic at nitrogen. The combination of the amphiphile **TACN** with **H** or **G** did not result in significant improvement in catalytic activity above the lead 1:4 **H**/**G** system.

Interestingly, the combination of the di-(2-picolyl)amine-containing amphiphile **DPA** with **H** in a 1:1 ratio in the presence of Zn^{2+} afforded significantly higher activity than the 1:4 **H**/**G** system (Figure 5a). The addition of **G** to give a 1:1:1 ratio of **H**/**G**/**DPA** afforded even higher activity, and reinforced the importance of the guanidium functional group, especially given that the concentration of the individual ligands in this combination are two-thirds of the concentrations found in the 1:1 **H**/**DPA** system. From these observations, we propose that the mechanism of esterolysis in the 1:1:1 **H**/**G**/**DPA** system proceeds via initial attack by the imidazole functionality in **H** to form histidine adduct **7** followed by attack of a hydroxide anion stabilized by a **DPA**·Zn^{2+} complex (Figure 5b). Mass spectrum analysis found evidence of histidine adduct **7** (see SI, section 4j). Both of the transition states in Figure 5b are stabilized by binding to **G**, which increases the electrophilicity of the carbonyl functional group and acts as an oxyanion hole.

The Michaelis-Menten parameters of the most effective catalyst systems, 1:4 **H**/**G** and 1:1:1 **H**/**G**/**DPA** were determined by measuring the initial rates of reaction at increasing concentrations of the substrate **PNPB** (Figure 6). The k_{cat} of 1:4 **H**/**G** and 1:1:1 **H**/**G**/**DPA** were determined to be $0.017 \pm 0.003\ s^{-1}$ and $0.023 \pm 0.006\ s^{-1}$ respectively, which are comparable to recently reported artificial esterases that predominantly involve well-defined rigid systems such as peptidic amyloids/fibrils,[24,30] catalysts immobilized onto solid-phase supports[17] and engineered proteins[61] (see table in Figure 6). The calculated k_{cat} values are also comparable to that of α-chymotrypsin ($0.016 \pm 0.002\ s^{-1}$),[62–64] although the catalytic efficiency (k_{cat}/K_M) of the enzyme ($3300 \pm 300\ M^{-1}s^{-1}$) is two orders of magnitude

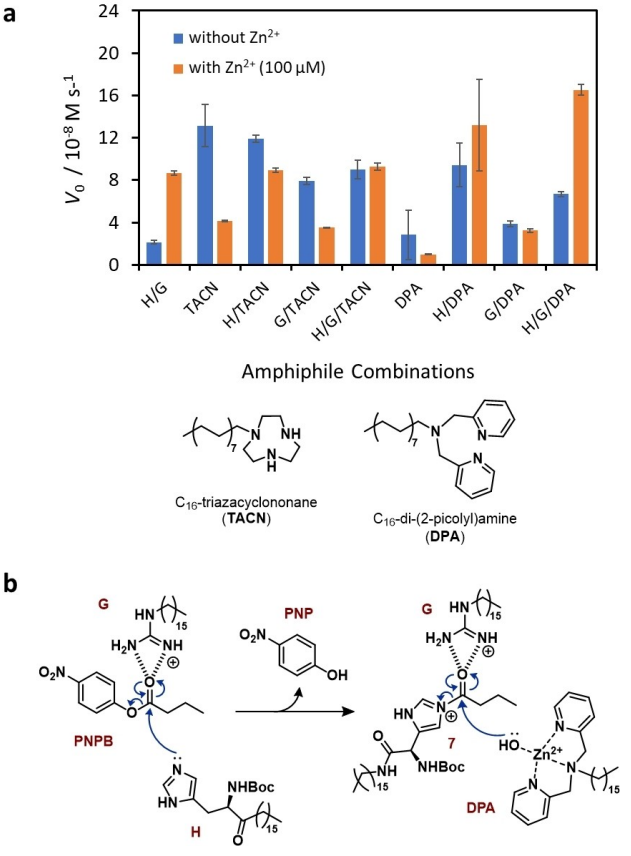

Figure 5. (a) Optimization screen in aqueous buffer pH = 7.0 ([HEPES] = 5 mM), [amphiphiles] = 100 μM, [**PNPB**] = 500 μM, 40 °C. (b) Proposed mechanism of esterolysis with the 1:1:1 **H**/**G**/**DPA** system.

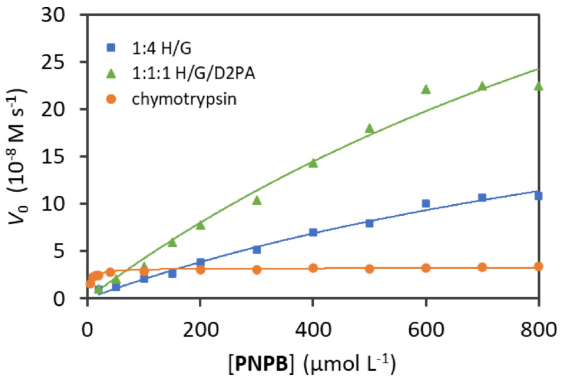

catalyst system	V_{max} (10^{-8} M s^{-1})	k_{cat} (s^{-1})	K_M (mM)	k_{cat}/K_M ($M^{-1}\ s^{-1}$)
1:4 **H/G**	33 ± 6	0.017 ± 0.003	1.5 ± 0.4	11 ± 5
1:1:1 **H/G/DPA**	75 ± 20	0.023 ± 0.006	1.7 ± 0.6	14 ± 9
MINP[32]		0.03	0.14	205
Ac-IHIHIQI-$CONH_2$[30]		0.026	0.4	62
Phe-His-C_{16}-SH[24]		0.016	1.4	11
Resin-triad[17]		0.027	12	2.3
TRI-peptide-[Zn^{2+}][61]		0.0054	1.7	3.1
α-chymotrypsin	3.20 ± 0.04	0.016 ± 0.002	0.0049 ± 0.0004	3300 ± 300

Figure 6. Michaelis-Menten fit for the rate of **PNPB** esterolysis for 1:4 **H**/**G** (100 μM, [Zn^{2+}] = 25 μM), 1:1:1 **H**/**G**/**DPA** (100 μM, [Zn^{2+}] = 25 μM), and α-chymotrypsin enzyme (2 μM, [$CaCl_2$] = 53 mM) in aqueous buffer pH 7.8 ([Tris] = 4 mM), 40 °C.

higher than 1:4 **H/G** ($11 \pm 5\ M^{-1}s^{-1}$) and 1:1:1 **H/G/DPA** ($14 \pm 9\ M^{-1}s^{-1}$). This shows that while our 1:4 **H/G** and 1:1:1 **H/G/DPA** systems may possess comparable activity at high substrate concentrations, significant advances still need to be made to compete with the specificity and efficiency of natural enzymes such as α-chymotrypsin. We also note that the activity parameters obtained from the Michaelis-Menten fit are likely afflicted by large errors due to the changing concentrations of the **PNPB**, which may alter the structure of the aggregates.

Some of the most efficient artificial esterases described to date are the molecularly-imprinted polymeric systems described by Zhao and co-workers,[32,33] which suggests that significant benefits can still be had from the generation of highly ordered structures. A possible approach to catalyst development in the future could be the combinatorial screening of amphiphilic molecules to identify novel groupings of catalytically active functional groups, followed by their immobilization onto solid supports or polymeric matrices.

Conclusions

In conclusion, we have demonstrated that the modular assembly of amphiphilic molecules can be used as a strategy for the screening and optimization of an artificial esterase. This approach involves the attachment of hydrophobic chains onto key functional groups that are known to participate synergistically in catalytic reactions. Unlike recent examples of the self-assembly of biomimetic catalysts that rely on the formation of nanofibrils and hydrogels, this strategy does not rely on specific molecular sequences within the building blocks; rather, the amphiphilic nature of the building blocks is what drives self-assembly. This greatly increases the flexibility of this strategy and allows it to be a platform for the future discovery of other biomimetic catalysts. It is important to note that the analysis of reaction rates while employing a combinatorial approach is complicated by the presence of multiple catalytic mechanisms. However, this can also be beneficial as screening can lead to catalytic systems not foreseen by rational design. The optimized artificial esterase developed in this study possesses a nucleophilic catalyst, an oxyanion hole and a metal ion chelator, and exhibits comparable efficiency (k_{cat}/K_M) to artificial systems featuring well-defined rigid binding pockets. Further advancements are required, however, to match the selectivity and efficiency of natural enzymes such as α-chymotrypsin. Current work in our group is focused on using a combinatorial strategy to screen for novel synergies from a wider range of functional groups, with a view to ultimately immobilizing the novel combinations onto solid supports for the generation of practically useful biomimetic catalysts.

Supporting Information Summary

The authors have cited additional references within the Supporting Information.[65,66]

Acknowledgements

The authors thank Dr Adrian Turner for assistance with TEM imaging. This work was supported by the MacDiarmid Institute for Advanced Materials and Nanotechnology. Olivia Matich thanks Auckland University of Technology for a Vice Chancellor's Doctoral Scholarship. Open Access publishing facilitated by Auckland University of Technology, as part of the Wiley - Auckland University of Technology agreement via the Council of Australian University Librarians.

Conflict of Interests

The authors declare no conflict of interest.

Data Availability Statement

The data that support the findings of this study are available from the corresponding author upon reasonable request.

Keywords: Amphiphiles · Biomimetic catalysis · Cooperative catalysis · Multifunctional catalysis · Self-assembly · Systems chemistry · Vesicles

[1] J.-M. Choi, S.-S. Han, H.-S. Kim, *Biotechnol. Adv.* **2015**, *33*, 1443–1454.
[2] R. DiCosimo, J. McAuliffe, A. J. Poulose, G. Bohlmann, *Chem. Soc. Rev.* **2013**, *42*, 6437–6474.
[3] A. J. T. Smith, R. Müller, M. D. Toscano, P. Kast, H. W. Hellinga, D. Hilvert, K. N. Houk, *J. Am. Chem. Soc.* **2008**, *130*, 15361–15373.
[4] A. J. Kirby, *Angew. Chem. Int. Ed. Engl.* **2003**, *35*, 706–724.
[5] M. T. Reetz, *Chem. Rec.* **2016**, *16*, 2449–2459.
[6] E. Kuah, S. Toh, J. Yee, Q. Ma, Z. Gao, *Chem. Eur. J.* **2016**, *22*, 8404–8430.
[7] M. Raynal, P. Ballester, A. Vidal-Ferran, P. W. N. M. van Leeuwen, *Chem. Soc. Rev.* **2014**, *43*, 1734–1787.
[8] K. I. Assaf, W. M. Nau, *Chem. Soc. Rev.* **2015**, *44*, 394–418.
[9] B. Soberats, E. Sanna, G. Martorell, C. Rotger, A. Costa, *Org. Lett.* **2014**, *16*, 840–843.
[10] Z. Dong, Q. Luo, J. Liu, *Chem. Soc. Rev.* **2012**, *41*, 7890–7908.
[11] J. Lagona, P. Mukhopadhyay, S. Chakrabarti, L. Isaacs, *Angew. Chem. Int. Ed.* **2005**, *44*, 4844–4870.
[12] A. Gissot, J. Rebek, *J. Am. Chem. Soc.* **2004**, *126*, 7424–7425.
[13] D. J. Cram, P. Y. S. Lam, S. P. Ho, *J. Am. Chem. Soc.* **2002**, *108*, 839–841.
[14] R. Breslow, S. D. Dong, *Chem. Rev.* **1998**, *98*, 1997–2012.
[15] S. Javor, E. Delort, T. Darbre, J.-L. Reymond, *J. Am. Chem. Soc.* **2007**, *129*, 13238–13246.
[16] E. Delort, T. Darbre, J.-L. Reymond, *J. Am. Chem. Soc.* **2004**, *126*, 15642–15643.
[17] M. D. Nothling, A. Ganesan, K. Condic-Jurkic, E. Pressly, A. Davalos, M. R. Gotrik, Z. Xiao, E. Khoshdel, C. J. Hawker, M. L. O'Mara, M. L. Coote, L. A. Connal, *Chem* **2017**, *2*, 732–745.
[18] P. Pengo, L. Baltzer, L. Pasquato, P. Scrimin, *Angew. Chem. Int. Ed.* **2007**, *46*, 400–404.
[19] P. Pengo, S. Polizzi, L. Pasquato, P. Scrimin, *J. Am. Chem. Soc.* **2005**, *127*, 1616–1617.
[20] L. Pasquato, F. Rancan, P. Scrimin, F. Mancin, C. Frigeri, *Chem. Commun.* **2000**, 2253–2254.
[21] S. Bal, K. Das, S. Ahmed, D. Das, *Angew. Chem. Int. Ed.* **2018**, *58*, 244–247.
[22] N. Singh, M. Kumar, J. F. Miravet, R. V. Ulijn, B. Escuder, *Chem. Eur. J.* **2016**, *23*, 981–993.
[23] C. Ghosh, S. Menon, S. Bal, S. Goswami, J. Mondal, D. Das, *Nano Lett.* **2023**, *23*, 5828–5835.
[24] N. Liu, S.-B. Li, Y.-Z. Zheng, S.-Y. Xu, J.-S. Shen, *ACS Omega* **2022**, *8*, 2491–2500.

[25] Y. Zhao, B. Lei, M. Wang, S. Wu, W. Qi, R. Su, Z. He, *J. Mater. Chem. B* **2018**, *6*, 2444–2449.
[26] M. Wang, Y. Lv, X. Liu, W. Qi, R. Su, Z. He, *ACS Appl. Mater. Interfaces* **2016**, *8*, 14133–14141
[27] C. Zhang, X. Xue, Q. Luo, Y. Li, K. Yang, X. Zhuang, Y. Jiang, J. Zhang, J. Liu, G. Zou, X.-J. Liang, *ACS Nano* **2014**, *8*, 11715–11723.
[28] I. W. Hamley, *Biomacromolecules* **2021**, *22*, 1835–1855.
[29] B. Sarkhel, A. Chatterjee, D. Das, *J. Am. Chem. Soc.* **2020**, *142*, 4098–4103.
[30] C. M. Rufo, Y. S. Moroz, O. V. Moroz, J. Stöhr, T. A. Smith, X. Hu, W. F. DeGrado, I. V. Korendovych, *Nat. Chem.* **2014**, *6*, 303–309.
[31] P. Makam, S. S. R. K. C. Yamijala, K. Tao, L. J. W. Shimon, D. S. Eisenberg, M. R. Sawaya, B. M. Wong, E. Gazit, *Nat. Catal.* **2019**, *2*, 977–985.
[32] I. Bose, F. Bahrami, Y. Zhao, *Mater. Today Chem.* **2023**, *30*, 101576.
[33] I. Bose, Y. Zhao, *ACS Catal.* **2021**, *11*, 3938–3942.
[34] M. D. Arifuzzaman, Y. Zhao, *ACS Catal.* **2018**, *8*, 8154–8161.
[35] C. Z. J. Ren, P. Solís-Muñana, G. G. Warr, J. L. Y. Chen, *ACS Catal.* **2020**, *10*, 8395–8401.
[36] C. Z. J. Ren, P. Solís Muñana, J. Dupont, S. S. Zhou, J. L. Y. Chen, *Angew. Chem. Int. Ed.* **2019**, *58*, 15254–15258.
[37] P. Solís Muñana, G. Ragazzon, J. Dupont, C. Z. J. Ren, L. J. Prins, J. L. Y. Chen, *Angew. Chem. Int. Ed.* **2018**, *57*, 16469–16474.
[38] M. Poznik, B. König, *Org. Biomol. Chem.* **2014**, *12*, 3175–3180.
[39] B. Gruber, E. Kataev, J. Aschenbrenner, S. Stadlbauer, B. König, *J. Am. Chem. Soc.* **2011**, *133*, 20704–20707.
[40] For key seminal work on functionalized surfactants, see references 40–43: F. Mancin, P. Scrimin, P. Tecilla, U. Tonellato, *Coord. Chem. Rev.* **2009**, *253*, 2150–2165.
[41] J. Zhang, X.-G. Meng, X.-C. Zeng, X.-Q. Yu, *Coord. Chem. Rev.* **2009**, *253*, 2166–2177.
[42] U. Tonellato, *Colloids Surf.* **1989**, *35*, 121–134.
[43] R. A. Moss, R. C. Nahas, S. Ramaswami, *J. Am. Chem. Soc.* **1977**, *99*, 627–629.
[44] W. Tagaki, M. Chigira, T. Amada, Y. Yano, *J. Chem. Soc. Chem. Commun.* **1972**, 219–220.
[45] T. Dwars, E. Paetzold, G. Oehme, *Angew. Chem. Int. Ed.* **2005**, *44*, 7174–7199.
[46] J. B. F. N. Engberts, *Pure Appl. Chem.* **1992**, *64*, 1653–1660.
[47] C. A. Bunton, G. Savelli, *Adv. Phys. Org. Chem.* **1986**, *22*, 213–309.
[48] T. Kunitake, S. Shinkai, *Adv. Phys. Org. Chem.* **1980**, *17*, 435–487.
[49] M. D. Nothling, Z. Xiao, N. S. Hill, M. T. Blyth, A. Bhaskaran, M.-A. Sani, A. Espinosa-Gomez, K. Ngov, J. White, T. Buscher, F. Separovic, M. L. O'Mara, M. L. Coote, L. A. Connal, *Sci. Adv.* **2020**, *6*, eaaz0404.
[50] M. D. Nothling, Z. Xiao, A. Bhaskaran, M. T. Blyth, C. W. Bennett, M. L. Coote, L. A. Connal, *ACS Catal.* **2018**, *9*, 168–187.
[51] N. J. V. Lindgren, L. Geiger, J. Razkin, C. Schmuck, L. Baltzer, *Angew. Chem. Int. Ed.* **2009**, *48*, 6722–6725.
[52] R. Ménard, A. C. Storer, *Biol. Chem. Hoppe-Seyler* **1992**, *373*, 393–400.
[53] T. G. Sprigings, C. D. Hall, *J. Chem. Soc. Perkin Trans. II* **2001**, 2063–2067.
[54] M. S. Han, D. H. Kim, *Bull. Korean Chem. Soc.* **2004**, *25*, 1151–1155.
[55] X. Liu, H. T. Ngo, Z. Ge, S. J. Butler, K. A. Jolliffe, *Chem. Sci.* **2013**, *4*, 1680–1686.
[56] J. Börner, I. dos Santos Vieira, U. Flörke, A. Döring, D. Kuckling and S. Herres-Pawlis, Zinc Complexes with Mono- and Polydentate Behaving Guanidine Ligands and Their Application in Lactide Polymerization, in *Renewable and Sustainable Polymers*, **2011**, pp. 169–200.
[57] H. Wittmann, V. Raab, A. Schorm, J. Plackmeyer, J. Sundermeyer, *Eur. J. Inorg. Chem.* **2001**, *2001*, 1937–1948.
[58] R. Feng, Y. Xu, H. Zhao, X. Duan, S. Sun, *Analyst* **2016**, *141*, 3219–3223.
[59] H. Fonge, L. Jin, J. Cleynhens, G. Bormans, A. Verbruggen, *Bioorg. Med. Chem.* **2010**, *18*, 396–402.
[60] Note that a high degree of error is associated with our calculated kcat and kcat/KM values due to the dynamic nature of the self-assembled system, where the nature of the aggregates can be altered by changes in the substrate concentration.
[61] M. L. Zastrow, A. F. A. Peacock, J. A. Stuckey, V. L. Pecoraro, *Nat. Chem.* **2011**, *4*, 118–123.
[62] N. Kundu, S. Roy, *Nature* **1970**, *226*, 1171–1171.
[63] G. W. Schwert, H. Neurath, S. Kaufman, J. E. Snoke, *J. Biol. Chem.* **1948**, *172*, 221–239.
[64] L. Anoardi, R. Fornasier and U. Tonellato, *J. Chem. Soc. Perkin Trans. 2* **1981**, 260–265.
[65] C. A. Bunton, F. Nome, F. H. Quina, L. S. Romsted, *Acc. Chem. Res.* **2002**, *24*, 357–364.
[66] E. D. Goddard, *Adv. Colloid Interface Sci.* **1974**, *4*, 45–78.

Manuscript received: June 3, 2024
Revised manuscript received: June 20, 2024
Accepted manuscript online: June 21, 2024
Version of record online: August 14, 2024